Real-time thickness and compositional control of $Ga_{1-x}In_xP$ growth using *p*-polarized reflectance

V. Woods[a] and N. Dietz
Department of Physics, North Carolina State University, Raleigh, North Carolina 27695

K. Ito and I. Lauko
Center for Research in Scientific Computation, North Carolina State University, Raleigh, North Carolina 27695

(Received 12 November 1999; accepted 27 March 2000)

Advances in the engineering and design of advanced electro-optical materials require sensors and control strategies that allow tight control over thickness and composition of multilayered structures. In response to this demand, we developed and applied *p*-polarized reflectance (PR) for real-time optical characterization and control of heteroepitaxial GaP/GaInP growth under pulsed chemical beam epitaxy conditions. For closed-loop control, we applied nonlinear control algorithms (based on nonlinear Kalman filtering) that utilizes the PR signals to adjust the source flows involved in the heteroepitaxial growth of $Ga_{1-x}In_xP$ on Si(001). A reduced order surface kinetics model has been formulated to establish the linkage between the surface reaction kinetic and its optical response. These data are linked to compute the compositional and thickness change per time unit, utilizing the monitored PR signals for validation. This allows the establishment of feedback control algorithms, able to control both the growth rate and composition of $Ga_{1-x}In_xP$ heterostructures. © *2000 American Vacuum Society.* [S0734-2101(00)12804-0]

I. INTRODUCTION

Recent developments in surface sensitive optical characterization techniques have made possible real-time monitoring of surface conditions during epitaxial growth. This information is of importance for systems employing chemical deposition processes for thin film growth, where changes in surface conditions greatly affect growth kinetics.[1,2]

This article presents advances in the utilization of *p*-polarized reflectance spectroscopy (PRS) as a link to control algorithms for the growth of III–V heterostructures under pulsed chemical beam epitaxy (PCBE) conditions. The high sensitivity of PRS towards surface conditions enables the real-time analysis and control of $Ga_{1-x}In_xP$/GaP growth.[3–5] During growth the surface of $Ga_{1-x}In_xP$/GaP heterostructures is periodically exposed to organometallic precursors which causes variations in the thickness and composition of the surface reaction layer (SRL). A reduced order surface kinetics (ROSK) model has been established to model the surface reaction kinetics with a reduced number of coupled differential equations.[6]

PRS is able to accurately probe changes in thickness and composition of the SRL, caused by the periodic supply of precursors employed to the surface. This information is linked to real-time estimation of instantaneous growth rate and composition using a virtual substrate model developed by Aspnes *et al.*[7]

II. EXPERIMENTAL SETUP

In order to characterize changes in the surface conditions of Ga_xIn_xP/GaP on Si(001) PRS and laser light scattering (LLS) have been incorporated by utilizing laser light beams ($\lambda_1 = 632.8$ and $\lambda_2 = 650$ nm) and Glan–Thompson prisms as shown schematically in Fig. 1. Two different angles of incident are utilized: the first angle of incidence is $\varphi_1 = 75.2°$ (PR_75) close to the psuedo-Brewster angle of the substrate and the second of $\varphi_2 = 71.5°$ (PR_70) close to the psuedo-Brewster angle of the growing film. LLS intensity is detected via a photomultiplier tube, placed 20° outside of the optical plane, in order to characterize surface roughening. Full consideration of experimental detail has been provided in a previous publication.[6]

During PCBE growth, the growth surface is periodically exposed to ballistic beams of tertiary-butylphosphine $[(C_4H_6)PH_2]$ (TBP), triethyl-gallium $[Ga(C_2H_5)_3]$ (TEG), and trimethyl-indium $[In(CH_3)_3]$ (TMI) at a growth temperature of 425–475 °C. The injection times and durations were kept constant as shown in Fig. 2. The flow of TBP is kept constant at 0.993 sccm to provide a phosphorous rich growth surface. The III–V flow ratio was maintained in the range of 1:20–1:40.

Figure 3 shows the signals from the PR and LLS detectors during the growth of GaP/$Ga_xIn_{1-x}P$ on Si(001). The growth process can be decomposed in four phases: (a) substrate and surface conditioning, (b) deposition of a GaP buffer layer, (c) growth of a compositionally graded $Ga_{1-x}In_xP$ heterostructure, and (d) deposition of a GaP cap layer. During substrate conditioning, the silicon wafer is heated approximately 500 °C with a continuous TBP flux employed at the surface after which the temperature is lowered to the growth temperature. A 250 Å GaP buffer layer is deposited on the silicon at temperature range from 425 to 475 °C. The $Ga_{1-x}In_xP$ heterostructure is then deposited on the GaP buffer layer. Figure 4 shows the target composition profile of such a het-

[a]Author to whom correspondence should be addressed; electronic mail: vtwoods@eos.ncsu.edu

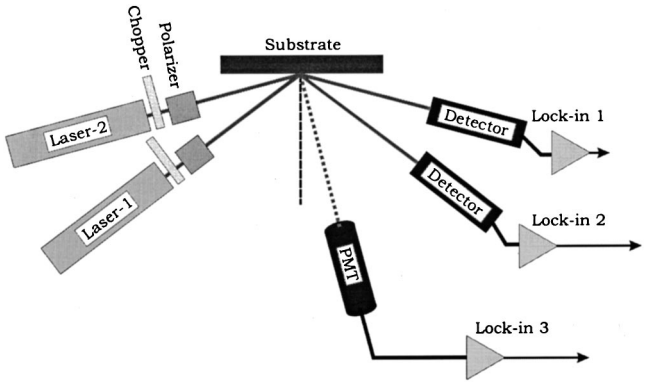

FIG. 1. Schematic setup of PRS and LLS for real-time growth monitoring.

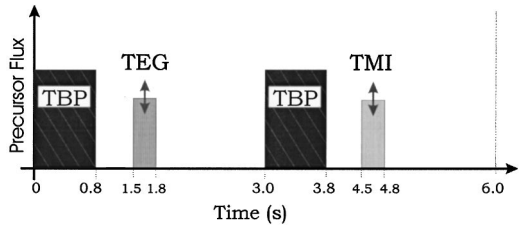

FIG. 2. Metalorganic precursor sequence. TBP flux is 0.993 sccm while TEG and TMI vary according to control algorithm.

erostructure and the PR signals at $\varphi=75°$ and $\varphi=70°$. In both Figs. 3 and 4, the large oscillations in the signals are due to the interference effect of the thin film growth. Superimposed on the interference fringes are fine structures that correspond to the periodic change of SRL constituents caused by the periodic employment of organometallic precursors to the SRL. The relative phase shift of the PR70 and PR75 signals is due to the difference in the angle of incidence and the psuedo-Brewster angle of the growing material. The psuedo-Brewster angle of silicon is approximately 75° while for $Ga_{1-x}In_xP$ it is between 71° and 74° (for an incident beam with a wavelength of 632.8 nm). A more detailed treatment of the correlation of the PR signal to the surface reaction layer can be found in a previous publication[6]

III. REDUCED ORDER SURFACE KINETICS MODEL AND CLOSED-LOOP CONTROL

The ROSK model for the binary compound semiconductor GaP growth from triethylgallium and tertiary-butylphosphine $[(C_4H_9)PH_2]$ has been discussed previously.[6] Treatment of the growth of $Ga_{1-x}In_xP$ from triethylgallium, tertiary-butylphosphine and trimethylindium has also been presented.[6]

The differential rate equations for the molar concentrations n_i of the SRL constituents in a $Ga_{1-x}In_xP$ system can be written as[6]

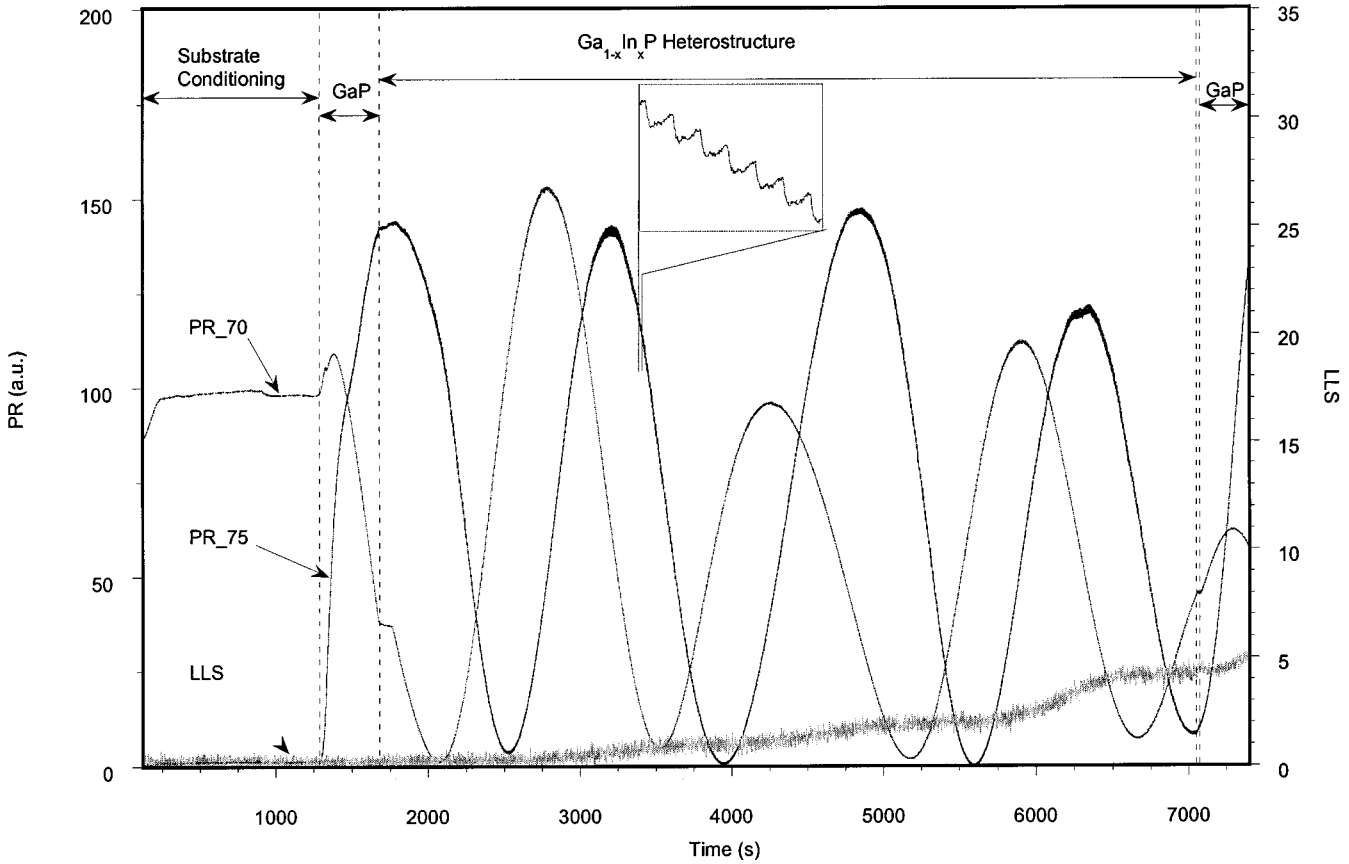

FIG. 3. Evolution of PR and LLS signals during GaP/$Ga_{1-x}In_xP$ growth on Si(001).

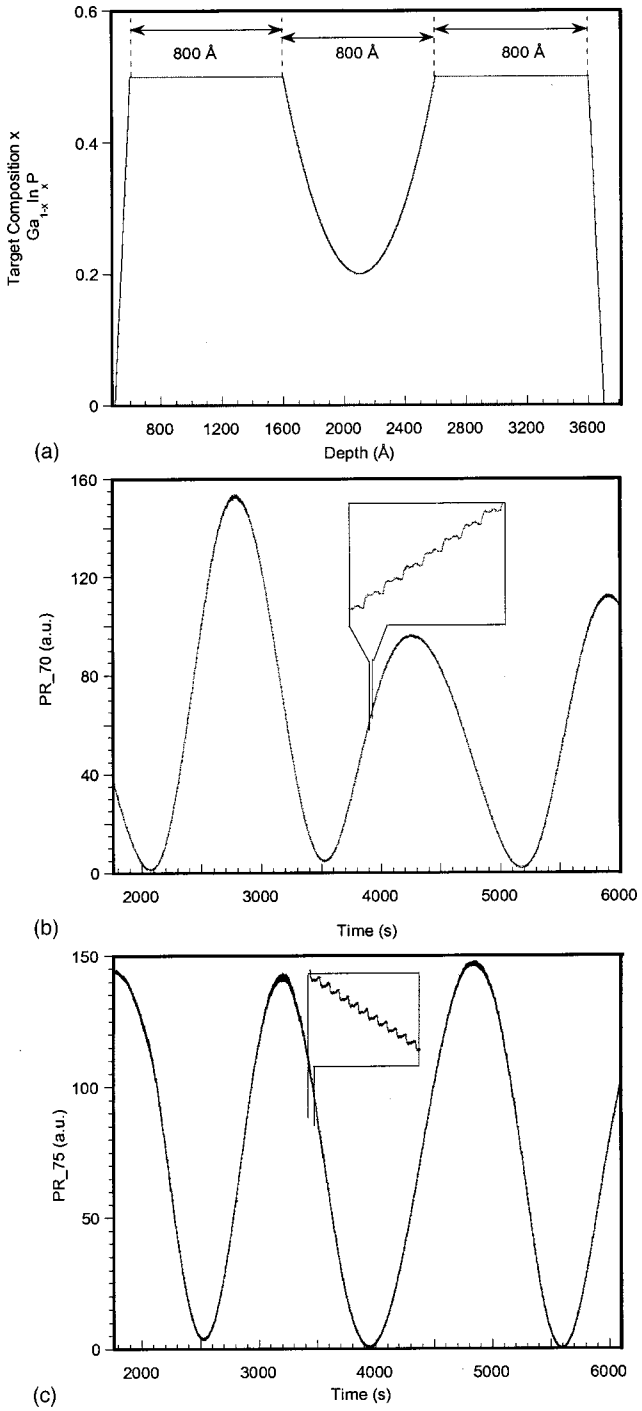

FIG. 4. $Ga_{1-x}In_xP$ heterostructure profile with PRS signal showing (a) desired compositional profile, (b) PR_70 signal, and (c) Pr_75 signal.

$$\frac{d}{dt}n_1 = n_{\mathrm{TBP}} - \hat{a}_1 n_1(t) - \hat{a}_4 n_3(t) n_1(t) - \hat{a}_7 n_6(t) n_1(t), \tag{1}$$

$$\frac{d}{dt}n_2 = n_{\mathrm{TEG}} - \hat{a}_2 n_2(t), \tag{2}$$

$$\frac{d}{dt}n_3 = \hat{a}_2 n_2(t) - \hat{a}_3 n_3(t) - \hat{a}_4 n_3(t) n_1(t), \tag{3}$$

$$\frac{d}{dt}n_5 = n_{\mathrm{TMI}} - \hat{a}_5 n_5(t), \tag{4}$$

$$\frac{d}{dt}n_6 = \hat{a}_5 n_5(t) - \hat{a}_6 n_6(t) - \hat{a}_7 n_6(t) n_1(t), \tag{5}$$

with the incorporation reactions for GaP and InP

$$\frac{d}{dt}n_4 = \hat{a}_4 n_3(t) n_1(t), \tag{6}$$

$$\frac{d}{dt}n_7 = \hat{a}_7 n_6(t) n_1(t), \tag{7}$$

respectively.

Equations (1)–(5) describe the reduced order TBP, TEG, and TMI pyrolysis as presented earlier. The formation of GaP and InP and their incorporation into the film are estimated by Eqs. (6) and (7).

The closed-loop control model employed, models the growth process as a four layer stack composed of the ambient/surface-reaction layer/film/substrate. The complex reflected amplitude of this multilayered stack may be obtained using a virtual substrate approach,[7–9] and can be written as

$$r = \frac{r_{01} - \hat{r}e^{-2i\Phi_1}}{1 + r_{01}\hat{r}e^{-2i\Phi_1}} \quad \text{with} \quad \hat{r} = \frac{r_{12} - r_k e^{-2i\Phi_2}}{1 + r_k e^{-2i\Phi_2}}. \tag{8}$$

The virtual reflection coefficients r_k are defined recursively for successive layers by

$$r_k = \frac{r_{k,k-1} - r_{k-1}e^{-2i\Phi_1}}{1 + r_{k,k-1}r_{k-1}\hat{r}e^{-2i\Phi_1}}, \quad r_k = A_k e^{-i\theta_k}. \tag{9}$$

Assuming that $|r_{01}|$, $|r_{12}|$, and $|\Phi_1|$ are sufficiently small, we approximate the reflected amplitude by

$$r \approx \frac{r_{02} + A_k e^{-(i\theta_k + 2\phi)}}{1 + A_k r_{02} e^{-21(\theta_k - \phi)}}, \tag{10}$$

where θ_k is the phase change per evaluation time unit due to the growth and ϕ is the phase change in the SRL due to modulation of SRL constituents and SRL thickness.

With this simplification, we are able to estimate the thickness of the bulk film, the growth rate of the each successive layer and the composition of these layers as

$$d_2 = \frac{\lambda}{4\pi\sqrt{\epsilon_2 - \epsilon_0 \sin^2 \varphi_0}}(\theta_{\mathrm{end}} - \theta_{\mathrm{begin}}), \tag{11}$$

$$gr_k = \frac{\lambda}{4\pi\sqrt{\epsilon_2 - \epsilon_0 \sin^2 \varphi_0}}(\theta_k - \theta_{k-1}), \tag{12}$$

and

$$x^k = \frac{gr^k_{\mathrm{InP}}}{gr^k_{\mathrm{GaP}} + gr^k_{\mathrm{InP}}}. \tag{13}$$

The growth of GaP and InP is determined in terms of the molar concentrations n_{GaP} and n_{InP} that are given through

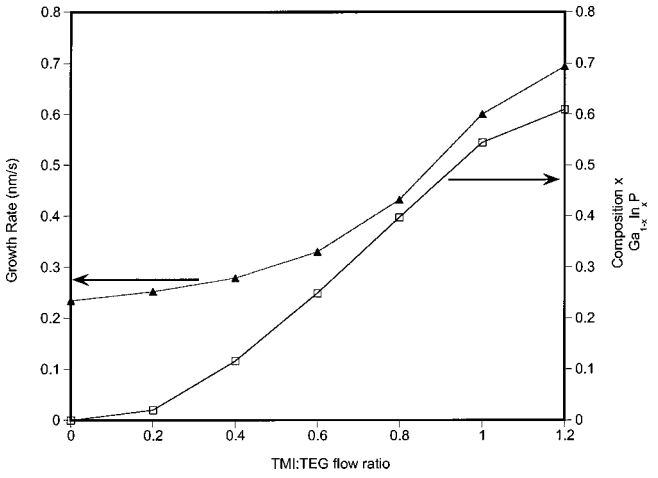

FIG. 5. Composition x and growth rate of $Ga_{1-x}In_xP$ as a function of TMI:TEG ratio.

$$\frac{dn_{GaP}}{dt} = k_4 n_P n_{Ga}, \tag{14}$$

and

$$\frac{dn_{InP}}{dt} = k_5 n_P n_{In}, \tag{15}$$

where n_P, n_{Ga}, and n_{In} denote the concentrations of surface active phosphorous, gallium, and indium, respectively. The rate constants k_4 and k_5 account for various surface kinetic processes as well as absorption/desorption processes from the growth surface. These rate constants are estimated in real time. Integration of Eq. (14) with respect to time results in

$$n_{GaP}(t_{k+1}) = e^{-C}[n_{GaP}(t_k) - S_{GaP}\mu_{TEG}] + S_{GaP}\mu_{TEG}, \tag{16}$$

where

$$C = k_4 \int_{t_k}^{t_{k+1}} n_P(t). \tag{17}$$

The input flow rates of μ_{TEG}^k and μ_{TMI}^k are determined by applying a nonlinear filtering algorithm,[10,11] and by minimizing the cost functions

$$\min_{u_{TEG}^k} |(1+z_k)n_{GaP}^+ - gr_d|^2 + \beta|\mu_{TEG}^k - \mu_{TEG}^{k-1}|^2, \quad \text{and} \tag{18}$$

$$\min_{u_{TEG}^k} \left| \frac{n_{InP}^+}{n_{GaP}^+} - \frac{z_k}{1-z_k} \right|^2 + \beta|\mu_{TMI}^k - \mu_{TMI}^{k-1}|^2, \tag{19}$$

which are subject to

$$n_{InP}^+ = e^{-C_{TMI}^K}(n_{InP}^C - S_{InP}u_{TMI}^k) + S_{InP}u_{TMI}^k, \tag{20}$$

and

$$n_{GaP}^+ = e^{-C_{TEG}^k}(n_{GaP}^C - S_{GaP}u_{TEG}^k) + S_{GaP}u_{TEG}^k. \tag{21}$$

C_{TEG}^k and C_{TMI}^k are the current estimate of the accumulated rate constant for GaP and InP cycle and z_k is the desired composition for the kth cycle.

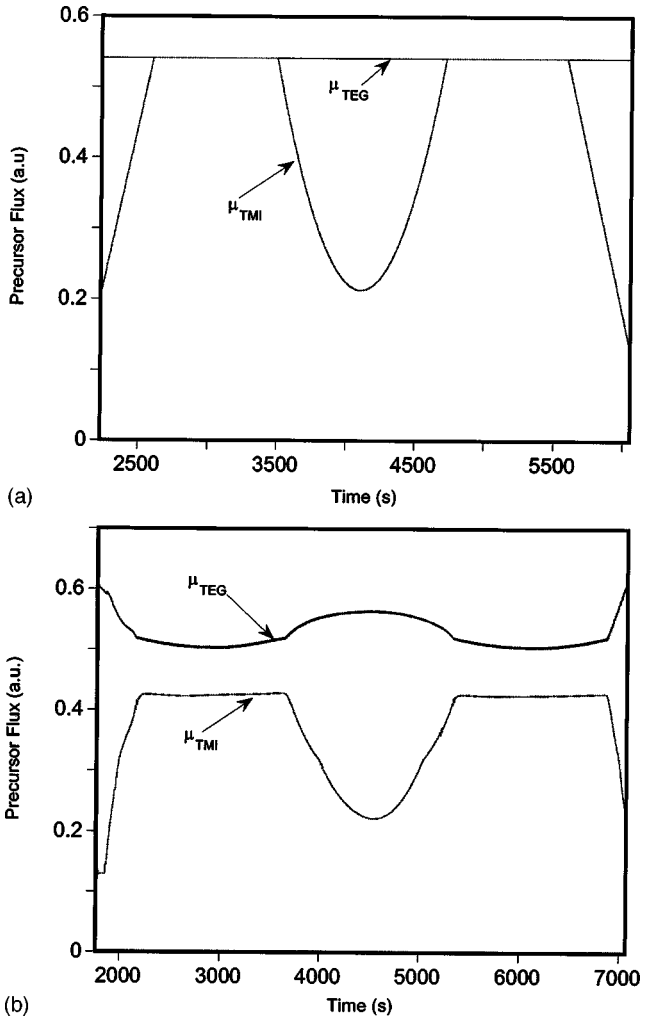

FIG. 6. (a) Precursor flux for open-loop control of $Ga_{1-x}In_xP$ quantum valve structure. (b) Precursor flux for closed-loop control.

IV. RESULTS: OPEN-LOOP AND CLOSED-LOOP RESULT

A series of experiments were conducted in order to compare the results of our closed-loop control algorithm to those of open-loop control. First, we established the correlation of composition and growth rate dependency as a function of flow ratio. For this correlation, a series of epilayers with thick constant composition x in $Ga_{1-x}In_xP$ were grown and analyzed by x-ray diffraction to obtain the compositional relationship with the established flow ratio TMI:TEG. The growth rates were estimated from the interference fringes obtained in the PR signals. The results of these *ex situ* analysis are summarized in Fig. 5. As shown, the growth rate and composition vary nonlinearly as a function of the flow ratio TMI:TEG. This effect may be due to the nonlinearity of the TMI flow controller for small flow settings, while for higher TMI flows the nonlinearity in the growth kinetics becomes dominant. The established correlation between growth rate and composition x with the TMI:TEG flow ratio is now used to grow compositionally graded heterostructures under both open-loop and closed-loop control conditions.

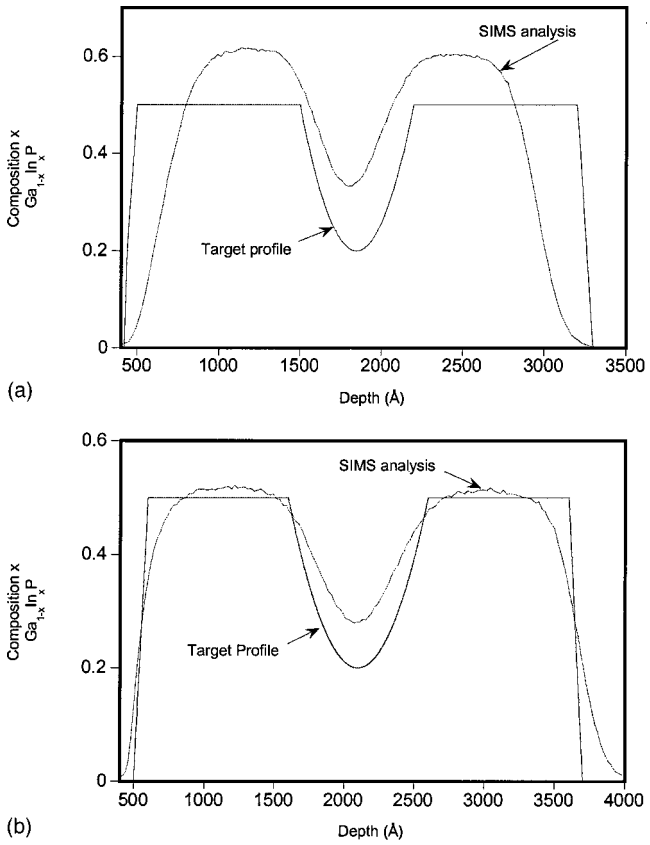

FIG. 7. (a) SIMS analysis of open-loop control $Ga_{1-x}In_xP$ heterostructure. (b) SIMS analysis of closed-loop control heterostructure.

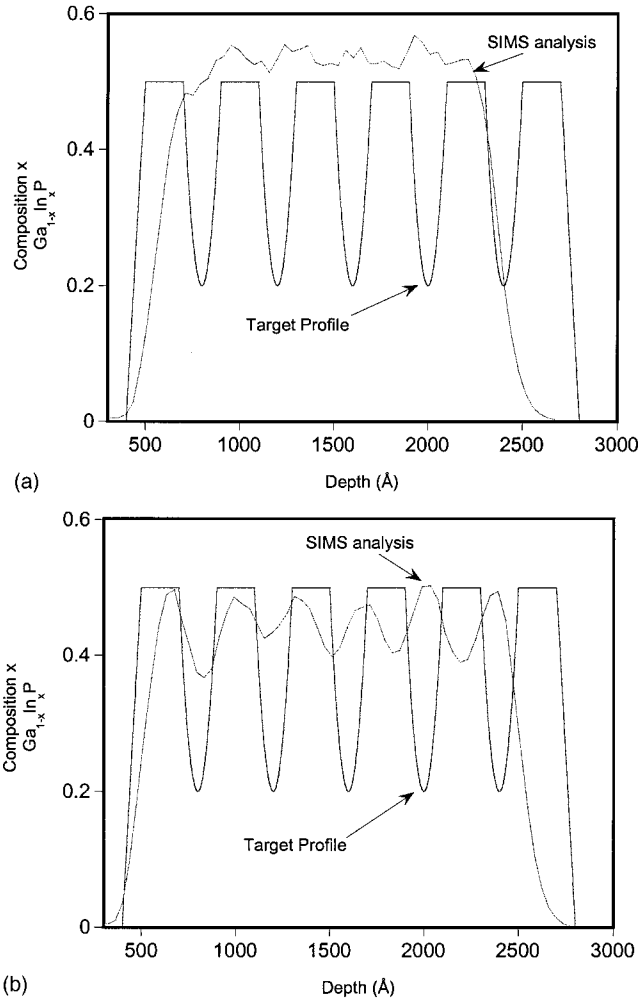

FIG. 8. (a) SIMS analysis of open-loop control of multiple quantum valve structure. (b) SIMS analysis of closed-loop control of multiple quantum valve $Ga_{1-x}In_xP$ structure.

The desired compositional profile shown in Fig. 4(a) was used for both open-loop and closed-loop control. For open-loop control, a predetermined time-wise flow profile, as shown in Fig. 6(a), was employed to grow these heterostructures in which the flow of TEG is kept constant and the flow of TMI is varied to match desired composition and thickness. The real-time updated closed-loop control flow profile is shown in Fig. 6(b). During closed-loop control, variation of the flow of TMI is employed to control composition x while variation in the flow of TEG is used to control the growth rate, as constrained by Eqs. (18)–(21). The on-line estimate of growth rate and composition provided by the PR probe adjusts to the nonlinearity in growth kinetics present in our system and provide better tracking to the desired profile.

Single and multiple quantum valve structures with thickness of 600 and 200 Å, respectively, were grown under both closed and open-loop control conditions as described earlier. Secondary ion mass spectroscopy (SIMS) analysis was employed to confirm composition and thickness of these samples. Figures 7 and 8 compare the results of the SIMS depth profile analysis for two parabolic graded heterostructures grown (a) under open-loop and (b) closed-loop control. For SIMS depth profiling, a primary Cs^+-ion beam was employed and the In^+–Cs and $^{71}Ga^{++}$–Cs-ion intensities detected. The sputtering rate varied from 2.46 to 4.23 Å/s, and is strongly compositionally dependent. Accounting for an instrumental broadening of approximately 50 Å and a depth integration of typically 40–50 Å, two errors in the SIMS analysis have to be considered: (a) the integration and instrumental broadening leads to a compositional smear out of profiles over 100–150 Å and (b) the compositional dependency of the sputtering rate leads to an accumulative error in the depth estimate. This error accumulation leads to large thickness uncertainties with increasing layer thickness. The instrumental broadening factor and the given integration time leads to an error in composition, estimated to be about 10%.

Figure 7 shows the compositional SIMS depth profile of a parabolic $Ga_{1-x}In_xP$ heterostructure under both (a) open-loop control and (b) closed-loop control. The discrepancy between the target profile and measured profile of the parabolic structure is attributed to the compositional smear out of SIMS data, as described before. The progressively poor tracking of the target profile at greater depths is related to the accumulative error associated with the compositionally dependent sputtering rate. Even though the SIMS analysis contains large error margins, it is clear that the closed-loop control algorithm displays superior tracking ability to the desired profile, particularly in maintaining a constant composition

both before and after the parabolic heterostructure.

Figure 8 shows the compositional SIMS depth profile for a grown multiple heterostructure, composed of a series of 200 Å parabolic $Ga_{1-x}In_xP$ wells separated by 200 Å of constant composition $x=0.50$ under both (a) open-loop and (b) closed-loop control. The SIMS analysis of these samples is also subject to the compositional smear out and the accumulative error in sputtering, which accounts for the shallow parabolic compositional structures and poor profile tracking at increasing depths. However, the comparison between open-loop and closed-loop control indicates that the closed-loop control maintains better profile tracking than the open-loop control algorithm.

The superior ability of the closed-loop control algorithm to track the desired compositional profile can be attributed to its capacity to adjust growth parameters to changing conditions in the reactor and in the surface reaction kinetics. These changes can lead to large variations in the rates of surface absorption and desorption of precursors,[1,2] greatly affecting growth characteristics. As shown in Fig. 5, the growth rate and composition x of $Ga_{1-x}In_xP$ are nonlinear with respect to TMI:TEG flow ratio. The ability in our closed-loop control algorithm to track in real-time thickness and composition supercedes these nonlinear growth behaviors. This ability to adjust instantaneously reduces calibration time required to grow different III–V heterostructures with high accuracy, leading to more efficient and varied output of epitaxial systems.

V. SUMMARY

We reported the compositionally and thickness controlled growth of $Ga_{1-x}In_xP$ in a PCBE reactor using PRS as a link to closed-loop feedback control. An online estimate of surface reaction kinetics, bulk film properties, growth rate, and instantaneous composition was obtained by integrating the PR signals and on-line control algorithms to adjust the flux of organometallic precursors TEG and TMI. The SIMS profile analysis showed the superiority of closed-loop control over open-loop for a series of $Ga_{1-x}In_xP$ quantum well structures.

ACKNOWLEDGMENT

This work has been supported by DOD-MURI Grant No. F49620-95-1-0447.

[1]S. M. Bedair *et al.*, J. Cryst. Growth **93**, 182 (1988).
[2]C. R. Abernathy, J. Vac. Sci. Technol. A **11**, 869 (1993); L. Niinist and M. Leskel, Thin Solid Films **225**, 130 (1993).
[3]N. Dietz and K. J. Bachmann, Mater. Res. Bull. **20**, 49 (1995).
[4]N. Dietz and K. J. Bachmann, Vacuum **47**, 133 (1996).
[5]N. Dietz, N. Sukidi, C. Harris, and K. J. Bachmann, J. Vac. Sci. Technol. A **15**, 807 (1997).
[6]N. Dietz, V. Woods, K. Ito, and I. Lauko, J. Vac. Sci. Technol. A **17**, 1300 (1999).
[7]D. E. Aspnes, J. Opt. Soc. Am. A **10**, 974 (1993).
[8]D. E. Aspnes, Appl. Phys. Lett. **62**, 343 (1993).
[9]D. E. Aspnes, US Patent No. 5,277,747 (1994).
[10]K. Ito and K. Ziong, Proc. IEEE (submitted).
[11]I. Lauko, K. Ito, V. Woods, and N. Dietz, J. Appl. Phys. (submitted).